Contents lists available at ScienceDirect

Chemical Engineering Research and Design

journal homepage: www.elsevier.com/locate/cherd

Disk structure on the performance of a rotating-disk dynamic filter: A case study on microalgae microfiltration

Kuo-Jen Hwang, Su-En Wu*

Department of Chemical and Materials Engineering, Tamkang University, Tamsui, New Taipei City 25137, Taiwan

ARTICLE INFO

Article history:
Received 18 August 2014
Received in revised form 28 October 2014
Accepted 9 December 2014
Available online 17 December 2014

Keywords:
Microfiltration
Rotating-disk filter
Microalgae concentration
Computational fluid dynamics

ABSTRACT

In a rotating-disk dynamic filter, the effects of the rotating-disk structure, including the shape and number of vanes, on the distribution of fluid velocity and shear stress acting on the membrane surface were examined using computational fluid dynamics (CFD). Six types of rotating disk were designed and installed above the filter membrane in a filter chamber to study their performance. Three-dimensional fluid flow fields in the filter chamber were simulated for various rotating disks, disk rotation speeds, and feed flow rates by using FLUENT software. The equations of continuity and momentum balance were solved numerically using a finite volume scheme along with the renormalization-group k–ε model. The simulated results indicated that the disk structure and rotation speed were the most crucial factors affecting the filtration performance. An optimal disk design for higher permeate fluxes and less membrane cake fouling can be achieved by increasing the shear stress on the membrane surface. A rotating disk equipped with more vanes can generate higher shear stress on the membrane surface for a given rotation speed. However, more power should be supplied to drive the rotating disk. Although the B2 rotating disk showed the highest filtration flux, Type-A2 and Type-C disks had the optimal designs, which were achieved by considering the filtration flux and power consumption simultaneously.
© 2014 The Institution of Chemical Engineers. Published by Elsevier B.V. All rights reserved.

1. Introduction

Microalgae are microscopic algae, often found in freshwater and marine environments. Because of their rapid growth and high lipid content, a range of microalgae species are produced in hatcheries and used for a variety of commercial purposes, for example, biodiesel production, health food preparation. The production of biodiesel from microalgae includes several stages, such as microalgae cultivation, microalgae concentration, cell disruption, and lipid extraction and purification (Chisti, 2007). Microfiltration has been increasingly used for microalgae concentration in recent years because it offers the advantages of high selectivity, low pollution, and energy saving. However, membrane fouling often unavoidably occurs during a filtration process. Comparing with conventional cross flow microfiltration, the high shear stress generated by a rotating-disk is more efficient in the mitigation of membrane fouling. Because microalgae always exhibit extremely high specific filtration resistance, using a rotating-disk filter to reduce cake formation is an effective method of enhancing the filtration flux.

A rotating-disk microfiltration module has been investigated for the purification and separation of various products, such as calcium carbonate (Bouzerar et al., 2000a,b), baker yeast (Brou et al., 2002), oil-in-water emulsion (Li et al., 2009), microalgae (Ríos et al., 2011; Hwang and Lin, 2014), and chicory juice (Zhu et al., 2013). Ríos et al. (2011) and Jaffrin et al. (2004) claimed that hydrodynamic parameters in a rotating-disk

* *Corresponding author*. Tel.: +886 2 26215656x2726; fax: +886 2 26209887.
E-mail address: kjhwang@mail.tku.edu.tw (K.-J. Hwang).
http://dx.doi.org/10.1016/j.cherd.2014.12.009
0263-8762/© 2014 The Institution of Chemical Engineers. Published by Elsevier B.V. All rights reserved.

Nomenclature

E_c	specific energy (power consumption per unit volume of received filtrate) (–)
k	velocity coefficient (–)
P	power consumption (kW)
Q	inlet feed flow rate (L/h)
q_s	pseudo-steady filtration flux (m^3/m^2s)
r	radial coordinate of analyzed system disk (m)
R_c	filtration resistance of cake (1/m)
R_m	filtration resistance of membrane (1/m)
t	filtration time (s)
T	torque (m^2kg/s)
w_c	cake mass (kg/m^2)
x	Cartesian coordinate used in analyzed system (m)
y	Cartesian coordinate used in analyzed system (m)
z	Cartesian coordinate used in analyzed system (m)

Greek letters

γ	local shear rate on the membrane surface (1/s)
γ_m	mean shear rate on the membrane surface (1/s)
μ	fluid viscosity (kg/s m)
ω	disk rotating speed (rpm)
ΔP	transmembrane pressure (Pa)
τ	local shear stress on the membrane surface (Pa)
τ_m	mean shear stress on the membrane surface (Pa)

module, such as the transmembrane pressure, rotation speed, fluid viscosity, and solute concentration, are major factors affecting the permeate flux. An increase in the rotation speed results in a higher shear rate and higher filtration flux. The maximum shear rate increased from 2.1×10^4 to 1.52×10^5 s^{-1} when the rotation speed of smooth disk increased from 500 to 1500 rpm (Jaffrin et al., 2004). Jaffrin (2008) reviewed various dynamic shear-enhanced filtration systems that generate membrane shear with the aid of rotating disks, vibrating disks, and vibrating membranes. The author noted that the flux is mainly governed by the maximum shear rate and can be increased to considerably high levels by increasing the rotation speed or vibration amplitude or by equipping the disk with large vanes. Lee et al. (1995) found that the shear rate at the membrane tip was as high as 1.2×10^5 s^{-1} at the maximum disk rotation speed of 3450 rpm. Previous studies (Bouzerar et al., 2000a,b; Brou et al., 2002; Jaffrin et al., 2004; Jaffrin, 2012; Zhu et al., 2013) have also proposed that equipping a rotating disk with vanes is beneficial for eliminating or mitigating membrane fouling and producing high permeate flux. However, the filtration rate and power consumption depend heavily on the structure of the rotating disk. The use of computational fluid dynamics (CFD) for designing a highly efficient rotating-disk filtration module is an effective, economical, and time-saving approach.

CFD is a useful method for simulating the velocity and shear stress distributions in a dynamic filtration system. Torras et al. (2006, 2009) used the commonly used CFD software FLUENT to simulate the pressure and shear stress distributions in the filter chamber for various rotation speeds and disk radii. Torras et al. (2009) used a standard *k-omega* turbulence model in the simulation for rotation speeds ranging from 300 to 20,000 rpm. The results were in agreement with previous experimental data. Hwang and Lin (2014) designed a rotating-disk filter chamber for microalgae concentration. The flow fields in the filter were simulated using the FLUENT software. The cake formation could be reasonably explained by the simulated shear stress distribution. An increase in the shear stress by two orders of magnitude, which was achieved by increasing the disk rotation speed, decreased the cake mass by 80% and enhanced the filtration flux by approximately 10 times.

In this study, to design an efficient rotating-disk for microalgae concentration, the distributions of fluid velocity and shear stress were simulated using CFD. Once the mean shear stress on the membrane surface was known, the cake mass and filtration flux were estimated based on empirical equations. The properties of microalgae cake were quoted directly from our previous study (Hwang and Lin, 2014) in the calculation. The optimal design of the rotating-disk was then determined from the viewpoints of high filtration flux and low power consumption.

2. Analyzed systems and numerical methods

2.1. Analyzed systems

A schematic diagram of the rotating-disk dynamic microfilter used in this study is shown in Fig. 1. Coordinates are also shown for the purpose of describing fluid flow directions. A rotating disk with a diameter of 145 mm was installed and connected to a rotating shaft driven by a motor. A filter membrane with a diameter of 155 mm was assembled on a porous support at the bottom. The width of the gap between the rotating disk and the membrane surface was 10 mm, and the diameters of the inlet and outlet conduits were both 10 mm. The feed flowed into the filter chamber from the inlet conduit near the top plate in the negative x-direction, the concentrate flowed out from the outlet conduit, and the filtrate flowed through the membrane and exited in the negative z-direction.

Six types of rotating disk were used, as shown in Fig. 2. Types A1 and A2 were both circular disks, with the only difference between them being the gap width between the disk and the membrane surface. The gap widths of Types A1 and A2 were 10 and 3 mm, respectively. Types B1 and C were equipped with two extra vanes with distinct shapes. The vanes of Type B1 had a uniform rectangular cross section, and those of Type C had a cross-sectional area that decreased in the outward direction from the disk center. The thickness, width, and length of the vanes for the Type-B1 disk were 6, 6, and 67 mm, respectively. The Type-B2 disk had four vanes with a shape identical to that of the Type-B1 disk. The Type-D disk had two vanes and two extra grooves; the vanes and grooves had the same cross-sectional areas as those of the Type-B1 disk and were arrayed in a staggered arrangement. The gap widths for these disks were all the same, except for Type A2.

2.2. Numerical methods

The GAMBIT software was used to plot the analyzed system, create the mesh for calculation, and set required boundary conditions. In a pretreatment process before the calculation, the main body structure and 3D meshes were created using unstructured hexahedral meshes. The total number of meshes was approximately 1,060,000 for all structures. The

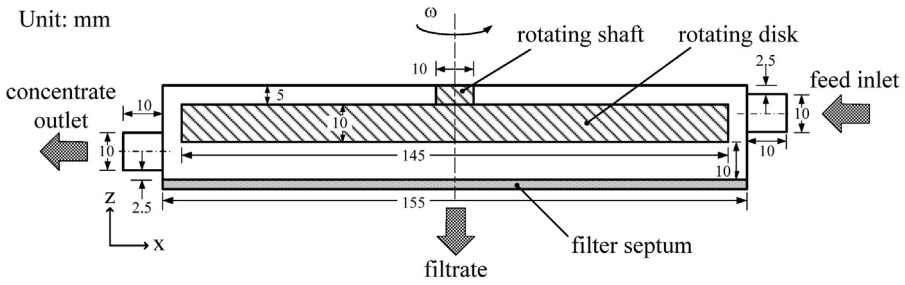

Fig. 1 – The filter chamber of a rotating-disk dynamic filter used in this study.

orthogonality of the grid lines, the aspect ratio, and the connectivity of the grids were automatically checked after mesh creation.

The fluid flow in the filter chamber was simulated using a segregated, steady-state, 3D implicit numerical solver in FLUENT Version 6.2. The governing equations were coupled using the SIMPLE algorithm, and the renormalization group k–ε model (RNG k–ε model) was employed for the turbulent flow. The RNG k–ε model was a turbulence model derived from the renormalization group theory (Yakhot and Orszag, 1986) and used for solving instantaneous Navier–Stokes equations. The two parameters in the model, turbulence kinetic energy (k) and its rate of dissipation (ε), were obtained from two transport equations. It is believed that the RNG k–ε model is more accurate and reliable than the standard k–ε model for a wider class of swirl flows. The boundary conditions included

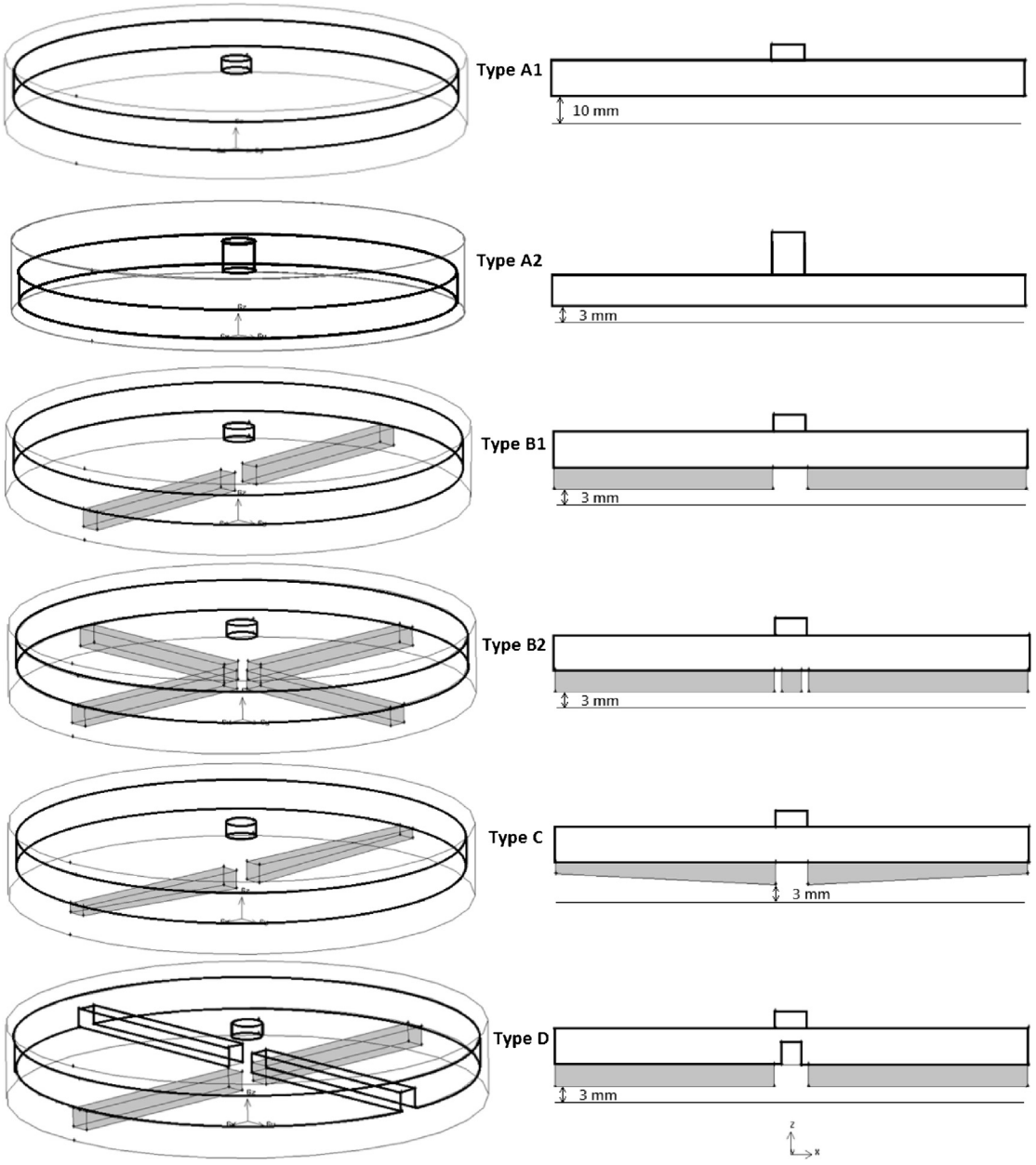

Fig. 2 – Schematic diagrams of different types of rotating-disks.

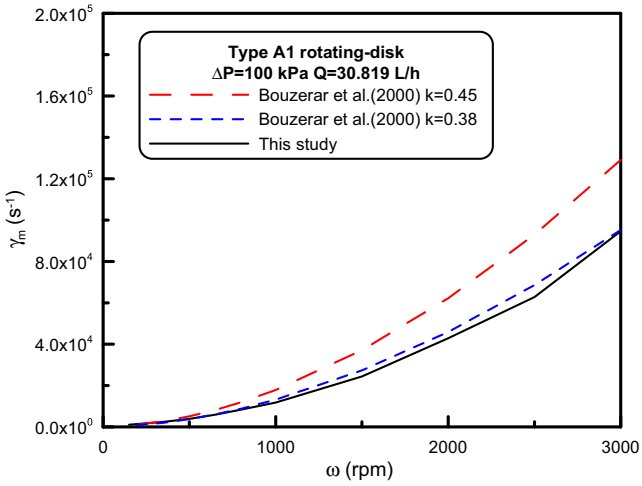

Fig. 3 – Comparisons of the mean shear rate between previous literature and this study under various rotating speeds.

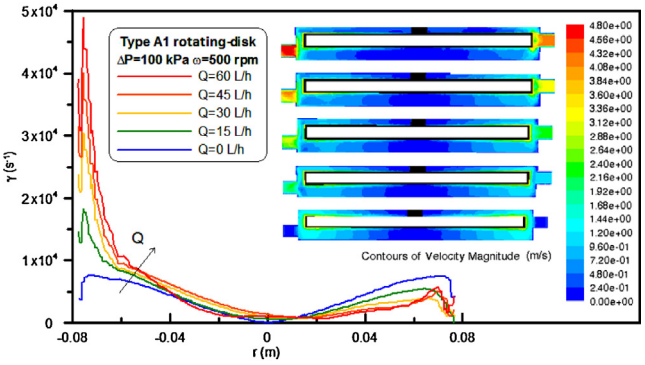

Fig. 4 – Distributions of shear rate on the membrane surface and fluid velocity on *xz*-plane at *y* = 0 for Type A1 rotating-disk at feed flow rates from 0 to 60 L/h.

one uniform velocity inlet and two constant-atmospheric-pressure outlets, and the conditions of all solid walls were set as nonslip. The convergence criteria were the residuals of continuity and velocity being below 10^{-5}.

2.3. *Materials*

A type of microalgae, *chlorella* sp., purchased from the Fisheries Research Institute, Council of Agriculture, Executive Yuan, Taiwan, was selected as a test sample. The microalgae cells had sizes ranging from 2 to 8 μm and a density of 1135 kg/m^3. The dispersion medium was liquid water, with a density of 998.2 kg/m^3 and a viscosity of 1.003×10^{-3} Pa s. The microalgae suspension concentration was 3.25 g/L. A hydrophilic filter membrane made of cellulose acetate ester and manufactured by ADVANTEC Co., Japan, was used as filter medium. The nominal mean pore size and filtration resistance of the membrane were 0.1 μm and 1.02×10^{11} m^{-1}, respectively. In this study, the experimental data of cake properties, including cake mass and specific filtration resistance, and filtration flux were quoted directly from our previous study using the rotating-disk of Type A1 (Hwang and Lin, 2014).

3. Results and discussion

Fig. 3 shows a comparison of the mean shear rates at the membrane surface between the values calculated using the empirical equation of Bouzerar et al. (2000a) with distinct empirical coefficients *k* and those obtained from simulations in the current study for various disk rotation speeds. The pressure at the filtrate exit and the feed flow rate were set as 100 kPa and 30.819 L/h, respectively. The coefficient *k* depends strongly on the disk geometry. According to published results (Bouzerar et al., 2000a,b; Jaffrin et al., 2004; Luo et al., 2013), the *k* value ranges from 0.30 to 0.45 for a plane disk, is exactly equal to 0.45 for a smooth disk, and is 0.84 for a disk with vanes. Because it is a function of disk geometry and cannot be obtained directly from theoretical derivations, it is better to determine by data fitting using the empirical equation proposed by Bouzerar et al. (2000a). Comparing the values of mean shear rates calculated using the empirical equation of Bouzerar et al. (2000a) with two *k* values with the simulation results of this study, the simulation results of this study were in agreement with the results of Bouzerar et al. (2000a) when *k* was set as 0.38, as shown in Fig. 3. The mean shear rate increased with the rotation speed because the fluid velocity profile near the membrane surface was steep. The mean shear rate obtained in this study ranged from 0 to 80,000 s^{-1}, which is similar to the values of Bouzerar et al. (2000a) under similar operating conditions. Thus, the method used in this study is reliable.

Fig. 4 shows the shear rate distribution on the membrane surface and the fluid velocity distribution in the *xz*-plane at *y* = 0 for the Type-A1 rotating disk for various feed flow rates. The pressure at the exits and the rotation speed were set to 100 kPa and 500 rpm, respectively. The fluid velocity in the filter chamber ranged from 0 to 4.8 m/s under these conditions. The fluid velocity was relatively high in regions near the surface of the rotating disk or in the inlet and outlet conduits, and it increased with the radial position because of the higher tangential velocity associated with a rotating disk. The highest velocity was observed near the rim of the rotating disk. By contrast, a low velocity was observed near the disk center. Furthermore, the shear rate increased with the radial coordinate because of a large velocity gradient in the gap between disk and the membrane surface. An asymmetrical shear rate distribution is observed on the membrane surface in Fig. 4, and similar results were obtained in a recent study of the present authors for a similar design (Hwang and Lin, 2014). The outlet conduit was closer to the membrane surface than the inlet, which resulted in a higher shear rate on the membrane surface near the outlet.

Fig. 5 shows the effects of the feed flow rate and rotation speed on the mean shear rate at the membrane surface for disk A1. An increase in the rotation speed leads to a higher mean shear rate, and this effect is more dominant at high rotation speeds. This is attributed to the steep velocity profile between the rotating disk and the membrane surface. By contrast, the feed flow rate exerts a small effect on the mean shear rate. This effect is negligible compared with that of the rotation speed.

Once the velocity profile is simulated using CFD, the shear rate on the membrane surface, which is the most crucial factor affecting cake formation, can be estimated. Fig. 6 shows the shear rate distributions on the membrane surface at *y* = 0 and *z* = 0 plane of the Type-A1 rotating disk for various rotation speeds from 1000 to 3000 rpm and a feed flow rate of 30.819 L/h. The outlet pressure was set to 100 kPa. The shear rate was approximately 0 at the center, increased toward the chamber walls (the maximum values were observed near the rim of the rotating disk), and then decreased drastically near

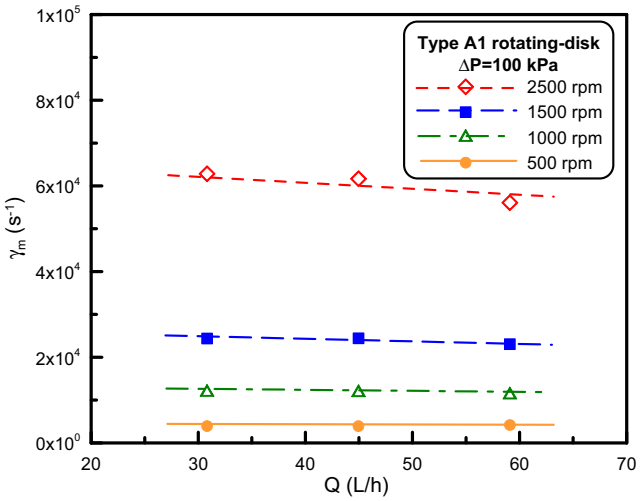

Fig. 5 – Effects of feed flow rate on the mean shear rate at four rotating speeds of Type A1 rotating disk.

the wall regions because of the no-slip condition on the wall. This trend can be explained reasonably from the fluid velocity profiles in Fig. 4. The shear rate distributions were slightly asymmetric because of the locations of the feed inlet and concentrate outlet. The shear rate near the feed inlet was lower than that at the concentrate outlet because the feed inlet was located at a higher level. A comparison of the curves in Fig. 6 indicates that an increase in the disk rotation speed leads to a higher shear rate, which is expected because of the considerable fluid velocity variation between the rotating disk and the membrane surface.

Fig. 7 shows the effect of the mean shear stress acting on the membrane surface on the cake mass and pseudosteady filtration flux for the Type-A1 rotating disk. The pressure exits and inlet feed flow rate were set to 100 kPa and 30.819 L/h, respectively. The mean shear stress was calculated from the CFD simulation data. The experimental data on the mean cake mass and filtration flux were obtained from Hwang and Lin (2014), who used a similar filter. The data on the cake mass versus shear stress relationship were regressed to a power relationship, as shown in Fig. 7. An increase in the shear stress leads to smaller cake mass because of the more significant sweeping effect occurring at the membrane

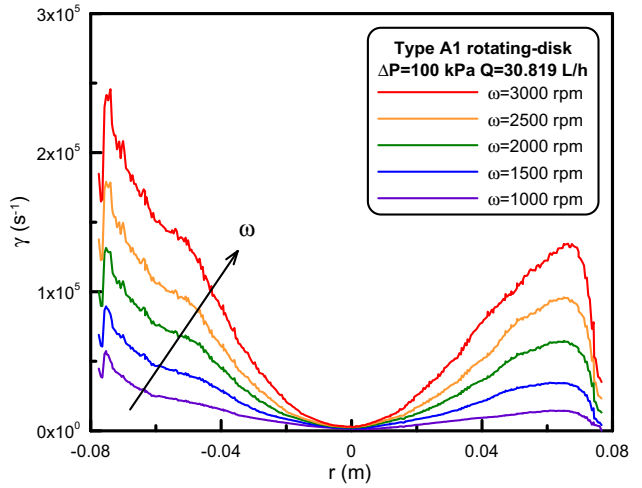

Fig. 6 – Shear rate distributions on membrane surface at y = 0 for Type A1 rotating-disk at disk rotating speeds from 1000 to 3000 rpm.

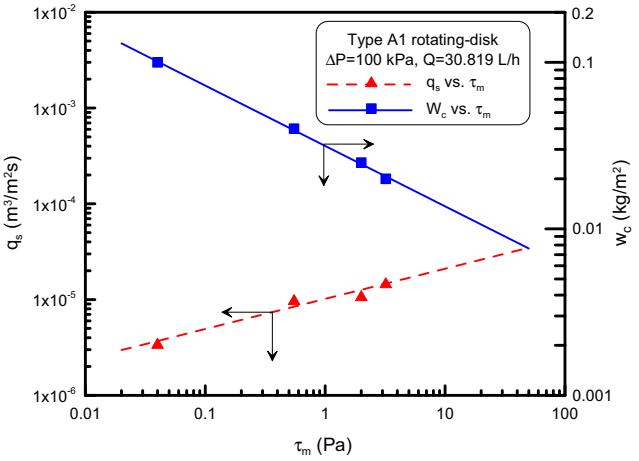

Fig. 7 – Effects of mean shear stress on the pseudo-steady filtration flux and mean cake mass for Type A1 rotating disk filter at Q = 30.819 L/h and ΔP = 100 kPa.

surface. The relationship between the mean shear stress and the cake mass can be expressed as

$$\ln\ w_c = -0.44 \ln \tau_m - 6.24 \quad (1)$$

The cake mass can decrease to one-twentieth of the original cake mass as the shear stress increases from 0 to 100 Pa. Furthermore, the pseudosteady filtration flux can be calculated using the basic filtration equation once the mean cake mass is known. The basic filtration equation based on the resistance-in-series model can be expressed as

$$q = \frac{\Delta P}{\mu(R_c + R_m)} = \frac{\Delta P}{\mu(w_c \cdot \alpha_{av} + R_m)} \quad (2)$$

where q is the filtration flux, ΔP is the transmembrane pressure, μ is the fluid viscosity, and R_c and R_m are the filtration resistances associated with cake formation and a clean membrane, respectively. The average specific cake filtration resistance α_{av} of microalgae is a power function of the transmembrane pressure, and the cake compressibility is 0.66 (Hwang and Lin, 2014). The calculated values of the filtration flux under various conditions are also shown as a curve in Fig. 7. A lighter cake formed under higher shear stress results in a higher filtration flux. The data shown in Fig. 7 also indicate that the cake mass and filtration flux can be estimated directly from the shear stress at the membrane surface.

Membrane fouling can be mitigated by inducing high shear stress on the membrane surface, which enhances the filtration flux. However, generating higher shear stress by increasing the disk rotation speed always involves more energy consumption as well as higher operation costs. The power required to drive a rotating disk can be estimated as

$$P = T\omega \quad (3)$$

where T is the torque. The torque of a rotating disk can be calculated as

$$T = \int_0^{2\pi}\int_0^{R} (-\tau_{z\theta} r)\big|_{z=H} r dr d\theta \quad (4)$$

where H is the gap width between the rotating disk and the membrane surface. Fig. 8 shows the power consumption and

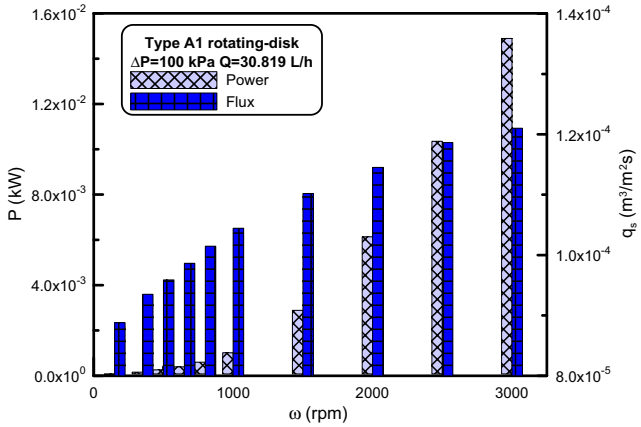

Fig. 8 – Effects of disk rotating speed on the power consumption and pseudo-steady filtration flux for Type A1 rotating disk filter at Q = 30.819 L/h and ΔP = 100 kPa.

pseudosteady filtration fluxes for various rotation speeds of the Type-A1 rotating disk. Although increasing the rotation speed leads to higher filtration flux because of higher shear stress acting on the membrane surface, the power consumption increases dramatically. A 36% increase in the filtration flux can be achieved by increasing the disk rotation speed from 150 to 3000 rpm. However, increasing the disk rotation speed to such a range requires 15 W of additional power. The filtration flux was markedly enhanced by increasing the disk rotation speed as $\omega < 1000$ rpm. When the disk rotation speed was higher, the increase in the filtration flux was small, and the power consumption increases drastically with the disk rotation speed. Therefore, it is more effective to operate the disk at a rotation speed lower than 1000 rpm from the viewpoint of saving energy.

The shear stresses at the membrane surface generated by various types of rotating disk were simulated to determine how the disk structure affects the filtration performance. Fig. 9 shows the shear stress distributions at the membrane surface for various rotating disks at a rotation speed of 3000 rpm. The pressure exits and inlet feed flow rate were set to 100 kPa and 30.819 L/h, respectively; and the disks were set to rotate counterclockwise. Type-A1 and Type-A2 rotating disks had no vanes, whereas Type B, Type C, and Type D were equipped with distinct numbers of vanes. The scale shown on the left indicates that the shear stress ranged from 0 (marked in navy blue) to 810 Pa (marked in bright red). The shear stress increased with the radial coordinate because of an increase in the tangential velocity of the rotating disk, and it reached the maximum values near the disk rim and just behind the vanes. Comparing the results for rotating disks with no vanes (Types A1 and A2), the shear stress can apparently be increased by reducing the gap width between the disk and the membrane. However, the magnitudes of shear stress were far smaller than those generated by disks equipped with vanes. In the presence of vanes, the distribution of shear stress was relatively asymmetrical; the influence of the inlet and outlet flows was negligible. A comparison of the results for Types B1 and B2 indicates that increasing the vane number can effectively improve the shear stress acting on the membrane surface, particularly in regions near the disk rim. The Type-D disk had a staggered arrangement of two convex vanes and two concave grooves. The shear stress generated by this disk was much lower than that generated by Type B2, and it was similar to but a little larger than that generated by Type B1. This observation implies that a groove can result in somewhat flowing turbulence, but generates shear stresses much smaller than those generated by a vane on the membrane surface. The two vanes on the Type-C rotating disk had cross-sectional areas decreasing in the radial direction; this caused the gap width between the vane edges and the membrane surface to increase. Consequently, the shear stress generated by the Type-C disk was smaller than that generated by the Type-B1 disk, although both had the same number of vanes. The shear stress was more uniformly distributed on the membrane surface for the Type-C rotating disk. Comparing all simulation results shown in Fig. 9, the shear stress can be observed to be the highest for Type B2 and the lowest for Type A1.

Fig. 10 shows a comparison of the power consumption and pseudosteady filtration flux among various types of rotating-disk filter at a rotation speed of 3000 rpm. The pressure exits and inlet feed flow rate were set to 100 kPa and 30.819 L/h, respectively. The power consumption and filtration flux were

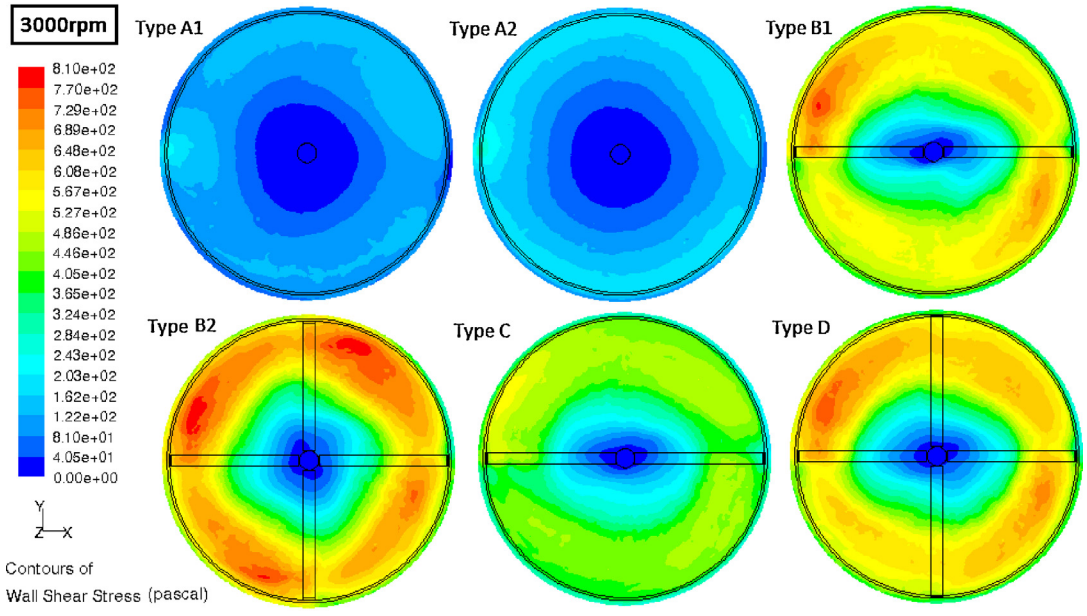

Fig. 9 – Shear stress distributions at the membrane surface for different types of rotating-disks under $\omega = 3000$ rpm.

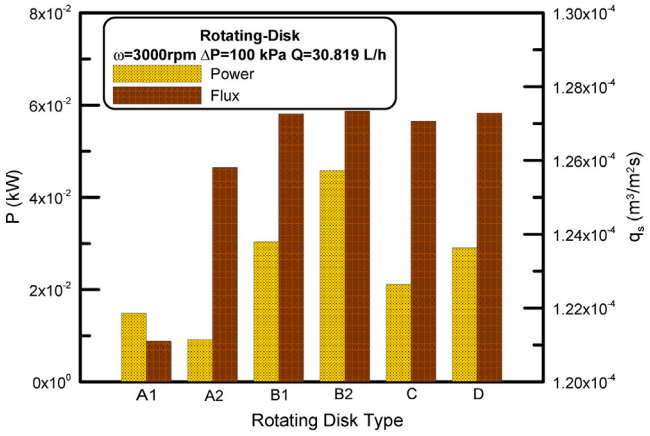

Fig. 10 – The power consumptions and pseudo-steady filtration fluxes for different types of rotating-disk filters at Q = 30.819 L/h and ΔP = 100 kPa.

strongly influenced by the rotating-disk structure. Equipping the disks with vanes or reducing the gap width between the disk and the membrane effectively enhanced the shear stress and improved the filtration flux. However, no significant difference in filtration flux was observed among disks equipped with vanes. This is because the cake mitigation effect becomes considerably small when the shear stress exceeds a certain value, as shown in Fig. 7. Furthermore, the power consumption was higher for rotating disks with vanes. A comparison of the Type-B1 and Type-B2 disks showed that the power consumption increased with the number of vanes. Both the Type-D and Type-B1 disks required nearly the same power. These two rotating disks also showed similar filtration performance. It is interesting that the Type-C disk showed lower power consumption compared with the other disks with vanes; the power consumption was only a half of that for Type B2 and three-fourths that for Type B1 and D.

Fig. 11 shows a comparison of the flux increase percentage on the basis of Type A1 between the various types of rotating disk for three distinct rotation speeds of 150, 500, and 3000 rpm. The pressure exits and inlet feed flow rate were set to 100 kPa and 30.819 L/h, respectively. Decreasing the gap width between the rotating disk and the membrane surface

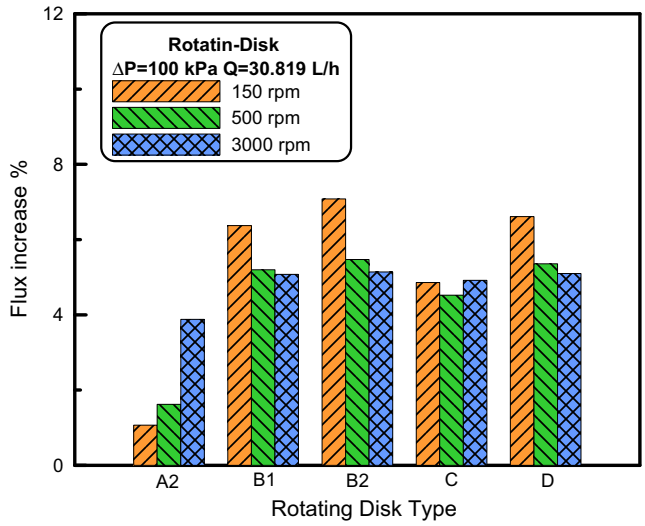

Fig. 11 – Comparisons of the flux increase rate among different types of rotating-disk filters at three disk rotating speeds, 150,500 and 3000 rpm (on the basis of Type A1).

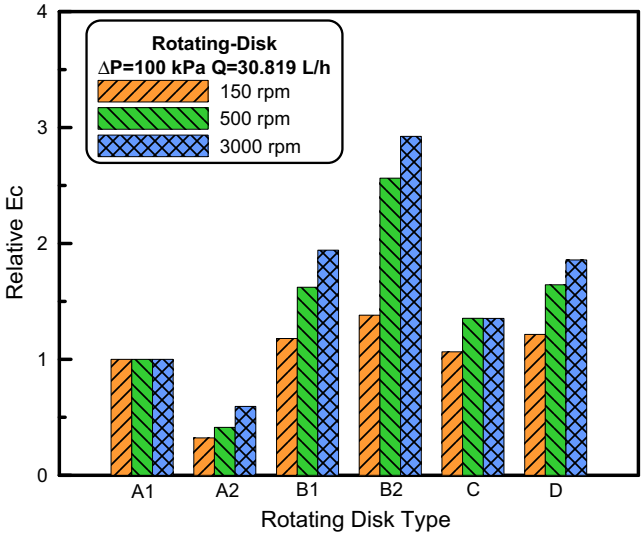

Fig. 12 – Comparisons of the relative specific energy among different types of rotating-disk filters at three disk rotating speeds, 150,500 and 3000 rpm (on the basis of Type A1).

(e.g., Type A2, is beneficial for flux improvement, particularly at higher rotation speeds). The filtration flux increased by 1.1% at ω = 150 rpm and by 3.9% at 3000 rpm. Equipping the rotating disk with vanes (Types B1, B2, C, and D) can enhance the filtration flux. This effect is more dominant for lower disk rotation speeds, except for Type C. The flux increase for the Type-C rotating disk was approximately 5% for various rotation speeds. The use of the Type-B2 disk results in the highest flux increase, 7.1% at a rotation speed of 150 rpm, because of the presence of several vanes. Unlike the filtration flux trend obtained for high disk rotation speeds, the flux difference among various rotating-disk types at a low rotation speed was more significant. The filtration flux sequence produced by the rotating disks at a rotation speed of 150 rpm was Type B2 > D > B1 > C > A2 > A1.

The specific energy is defined as the power consumption per unit volume of the received filtrate (Luo et al., 2010). Fig. 12 shows a comparison of the relative specific energy between the various types of filter and based on the data of Type A1, at three distinct disk rotation speeds. The pressure exits and inlet feed flow rate were set to 100 kPa and 30.819 L/h, respectively. All rotating disks exhibited higher specific energy compared with Type A1. The data revealed that the power consumption for obtaining a unit volume of filtrate was higher at higher rotation speeds. The specific energy increased with the rotation speed. Comparing the data on the specific energy of the rotating disks equipped with vanes for a given rotation speed, the Type-B2 disk showed the highest specific energy, Types B1 and D showed similar behavior, Type C showed a lower specific energy, and Type A2 showed the lowest value. Comparing the results shown in Figs. 8–12, the Type-A2 and Type-C rotating disks showed the optimal designs for microalgae concentration because they resulted in relatively high filtration fluxes and showed low power consumption.

4. Conclusion

The distribution of fluid velocity and shear stress acting on the membrane surface were simulated using the FLUENT software. The fluid velocity increased with the radial position because of the high tangential velocity associated with a

rotating disk. The highest velocity was observed near the rim of the rotating disk. The fluid velocity was relatively high in regions near the surface of the rotating disk or in the inlet and outlet conduits. An increase in the disk rotation speed led to a higher shear rate and reduced cake formation. The cake mass was correlated empirically with the mean shear stress and used for flux estimation. Although an increase in the disk rotation speed resulted in higher filtration flux, the power consumption increased dramatically. Therefore, it is more effective to operate the disk at a rotation speed lower than 1000 rpm for microalgae concentration from the viewpoint of saving energy.

The power consumption and filtration flux were determined mainly by the rotating-disk structure, except for the rotation speed. Equipping the disk with vanes or reducing the gap width between the disk and membrane were effective in enhancing the shear stress as well as in improving the filtration flux. The Type-C disk required the lowest power consumption compared with the other disks with vanes, only half of the power required by Type B2 and three-fourth of that required by Types B1 and D. The filtration flux amount produced by the rotating disks at a rotation speed of 150 rpm was in the order Type B2 > D > B1 > C > A2 > A1. A comparison of the results for various rotating disks showed that Type-A2 and Type-C rotating disks had the optimal designs for microalgae concentration because they resulted in relatively high filtration fluxes and showed low power consumptions. In conclusion, this study provided an effective method for the design and optimized operation of rotating-disk dynamic filter.

Acknowledgement

The authors wish to express their sincere gratitude to the Ministry of Science and Technology of the Republic of China for its financial support (Grant number: NSC102-2221-E-032-040).

References

Bouzerar, R., Ding, L., Jaffrin, M.Y., 2000a. Local permeate flux–shear–pressure relationships in a rotating disk microfiltration module: implications for global performance. J. Membr. Sci. 170 (1), 127–141.

Bouzerar, R., Jaffrin, M.Y., Ding, L., Paullier, P., 2000b. Influence of geometry and angular velocity on performance of a rotating disk filter. AIChE J. 46 (2), 257–265.

Brou, A., Ding, L., Boulnois, P., Jaffrin, M.Y., 2002. Dynamic microfiltration of yeast suspensions using rotating disks equipped with vanes. J. Membr. Sci. 197, 269–282.

Chisti, Y., 2007. Biodiesel from microalgae. Biotechnol. Adv. 25, 294–306.

Hwang, K.J., Lin, S.J., 2014. Filtration flux–shear stress–cake mass relationships in microalgae rotating-disk dynamic microfiltration. Chem. Eng. J. 244, 429–437.

Jaffrin, M.Y., 2008. Dynamic shear-enhanced membrane filtration: a review of rotating disks, rotating membranes and vibrating systems. J. Membr. Sci. 324 (1–2), 7–25.

Jaffrin, M.Y., 2012. Dynamic filtration with rotating disks, and rotating and vibrating membranes: an update. Curr. Opin. Chem. Eng. 1, 1–7.

Jaffrin, M.Y., Ding, L., Akoum, O., Brou, A., 2004. A hydrodynamic comparison between rotating disk and vibratory dynamic filtration systems. J. Membr. Sci. 242 (1–2), 155–167.

Lee, S.A., Russoti, B.G., Buckland, B., 1995. Microfiltration of recombinant yeast cells using a rotating disk dynamic filtration system. Biotechnol. Bioeng. 48, 386–400.

Li, L., Ding, L., Tu, Z., Wan, Y., Clausse, D., Lanoisellé, J.-L., 2009. Recovery of linseed oil dispersed within an oil-in-water emulsion using hydrophilic membrane by rotating disk filtration system. J. Membr. Sci. 342, 70–79.

Luo, J., Ding, L., Wan, Y., Paullier, P., Jaffrin, M.Y., 2010. Application of NF-RDM (nanofiltration rotating disk membrane) module under extreme hydraulic conditions for the treatment of dairy wastewater. Chem. Eng. J. 163, 307–316.

Luo, J., Zhu, Z., Ding, L., Bals, O., Wan, Y., Jaffrin, M.Y., Vorobiev, E., 2013. Flux behavior in clarification of chicory juice by high-shear membrane filtration: evidence for threshold flux. J. Membr. Sci. 435, 120–129.

Ríos, S.D., Clavero, E., Salvadó, J., Farriol, X., Torras, C., 2011. Dynamic microfiltration in microalgae harvesting for biodiesel production. Ind. Eng. Chem. Res. 50, 2455–2460.

Torras, C., Pallarès, J., Garcia-Valls, R., Jaffrin, M.Y., 2006. CFD simulation of a rotating disk flat membrane module. Desalination 200, 453–455.

Torras, C., Pallares, J., Garcia-Valls, R., Jaffrin, M.Y., 2009. Numerical simulation of the flow in a rotating disk filtration module. Desalination 235 (1–3), 122–138.

Yakhot, V., Orszag, S.A., 1986. Renormalization group analysis of turbulence: I. Basic theory. J. Sci. Comput. 1 (1), 1–51.

Zhu, Z., Luo, J., Ding, L., Bals, O., Jaffrin, M.Y., Vorobiev, E., 2013. Chicory juice clarification by membrane filtration using rotating disk module. J. Food Eng. 115 (2), 264–271.